

**Lifetimes of the first excited  $2^+$  states in  $^{176,178,180}\text{Os}$** O. Möller,<sup>1</sup> P. Petkov,<sup>1,2</sup> B. Melon,<sup>1</sup> A. Dewald,<sup>1</sup> A. Fitzler,<sup>1</sup> J. Jolie,<sup>1</sup> D. Tonev,<sup>3</sup> S. Christen,<sup>1</sup> B. Saha,<sup>1</sup> K. O. Zell,<sup>1</sup> and M. Heidemann<sup>1</sup><sup>1</sup>*Institut für Kernphysik der Universität zu Köln, D-50937 Köln, Germany*<sup>2</sup>*Bulgarian Academy of Sciences, Institute for Nuclear Research and Nuclear Energy, BG-1784 Sofia, Bulgaria*<sup>3</sup>*Instituto Nazionale di Fisica Nucleare, Laboratori Nazionali di Legnaro, Legnaro, Italy*

(Received 24 January 2005; published 23 September 2005)

By use of the pulsed-beam technique, the lifetimes of the first excited  $2^+$  states in  $^{176,178}\text{Os}$  were measured for the first time and the lifetime of the  $2_1^+$  state in  $^{180}\text{Os}$  was determined to a greater accuracy. In addition, for  $^{178}\text{Os}$ , a recoil-distance Doppler-shift experiment and an experiment to measure the nuclear deorientation effect that is due to the hyperfine interactions were also performed. The results obtained from this measurement are consistent with the lifetime value extracted by means of the pulsed-beam experiment. As well, the lifetimes of two  $I^\pi = 7^-$  isomers in  $^{180}\text{Os}$  were determined more accurately. Together with previously published data for the even-even osmium isotopes, the newly determined  $B(E2, 2_1^+ \rightarrow 0_1^+)$  transition strengths show a maximum value at the  $N = 104$  midshell. This maximum corresponds to the simple expectation of the  $N_\pi N_\nu$  rule of the interacting boson approximation (IBA) but remains to be explained by microscopic models.

DOI: [10.1103/PhysRevC.72.034306](https://doi.org/10.1103/PhysRevC.72.034306)

PACS number(s): 21.10.Tg, 23.20.Lv, 27.70.+q

**I. INTRODUCTION**

The lifetimes of the first excited  $2^+$  states in even-even nuclei provide an important piece of information on the quadrupole deformation  $\beta$  of the nuclear shape [1]. The value of  $\beta$  (hereafter we identify  $\beta$  and  $\beta_2$ ) experimentally determined from the  $B(E2, 2_1^+ \rightarrow 0_1^+)$  transition strength can be used to make a comparison with theoretical calculations based on different approaches and especially on microscopic ones. It is well known that the quadrupole deformation is one of the important factors which determines the properties of nuclear binding energies and nuclear excited states. Therefore the experimental systematics of quadrupole deformation has a deep impact on the understanding of nuclear structure and its evolution as a function of the valence nucleons.

At present, considerable effort has been made to explore the development of nuclear deformation in regions far from stability in order to test the persistence of well-established shell closures at extreme isospin values. For such investigations, reliable and complete experimental data, e.g., low-lying energies of excited states and  $B(E2)$  values, are required for various regions of the nuclear chart in order to distinguish local deviations from general trends.

R. F. Casten proposed a simple relation for the description of the  $B(E2, 0_1^+ \rightarrow 2_1^+)$  values in even-even nuclei as a function of valence neutrons  $N_\nu$  and valence protons  $N_\pi$ , where the leading term is the product  $N_\nu N_\pi$  [2]. According to this relation,  $B(E2, 0_1^+ \rightarrow 2_1^+)$  values are expected to increase when going from the closed shell at  $N = 82$  toward midshell, where maximum values are expected. From midshell toward the shell closure at  $N = 126$ , the  $B(E2, 0_1^+ \rightarrow 2_1^+)$  values are expected to decrease. Consequently, for the Os nuclei, maximal values are expected at  $N = 104$ .

Our purpose in the present work was to perform lifetime measurements in even-even  $^{176-180}\text{Os}$  by using the delayed-coincidence method with a pulsed beam to determine the lifetimes of the  $2_1^+$  levels in these nuclei. Before the present

investigation, lifetime information for these levels was available only for  $^{180}\text{Os}$  and no lifetime measurements had been performed for  $^{176,178}\text{Os}$ . To cross-check the results obtained from the delayed-coincidence experiments, we also carried out a recoil-distance Doppler-shift (RDDS) measurement for  $^{178}\text{Os}$ .

**II. EXPERIMENTS**

All experiments presented in this work were performed at the FN tandem accelerator at the University of Cologne. Excited states in  $^{176,178,180}\text{Os}$  were populated by means of  $^{164,166,168}\text{Er}(^{16}\text{O}, 4n)$  reactions at a beam energy of 80 MeV. For the electronic timing experiments, a pulsed  $^{16}\text{O}$  beam of 2.6-ns full-width at half-maximum (FWHM) was supplied. Enriched  $^{164,166,168}\text{Er}$  targets, evaporated onto a Au backing, were used. Further details on the targets are summarized in Table I. In the measurements for  $^{178,180}\text{Os}$  an additional 1.6 mg/cm<sup>2</sup> Ta foil was mounted directly behind the Au backing (see subsequent discussion). Deexciting  $\gamma$  rays were detected by a low-energy-photon (LEP) Ge detector of 22-cm<sup>3</sup> volume, positioned at  $0^\circ$  with respect to the beam axis. An overall time resolution of 10 ns was obtained at a  $\gamma$ -ray energy of 130 keV for this detector. The recorded events were sorted offline in time- $\gamma$ -ray-energy matrices. Measured time spectra are presented in Fig. 1 together with the corresponding prompt reference-time spectra.

In addition, for  $^{178}\text{Os}$  two more experiments were performed, again with the  $(^{16}\text{O}, 4n)$  reaction. The first was a RDDS measurement for which the Cologne plunger apparatus [3] was used. Singles spectra were measured with the LEP detector at  $0^\circ$  and a second Ge detector positioned at  $140^\circ$  with respect to the beam axis at target-to-stopper distances of 10, 100, 300, 600, 1000, 1500, 2000, 2500, 3000, 4000, 5000, 6000, 7300, and 12,000  $\mu\text{m}$ . Energy resolutions of 0.7 and 1.1 keV at a  $\gamma$ -ray energy of  $E_\gamma = 130$  keV were obtained

TABLE I. Details on the delayed-coincidence measurements. An additional separate 1.6 mg/cm<sup>2</sup> Ta foil was used in the experiments for <sup>178,180</sup>Os.

Reaction	$E(^{16}\text{O})$ (MeV)	Target (mg/cm <sup>2</sup> )	Enrichment (%)	Backing (mg/cm <sup>2</sup> )
<sup>164</sup> Er( <sup>16</sup> O, 4n) <sup>176</sup> Os	80	1.1	62.4(24.3% <sup>166</sup> Er)	Au, 1.9
<sup>166</sup> Er( <sup>16</sup> O, 4n) <sup>178</sup> Os	80	1.7	95.5	Au, 1.9
<sup>168</sup> Er( <sup>16</sup> O, 4n) <sup>180</sup> Os	80	1.1	98.3	Au, 2.0

for the LEP detector and the second Ge detector, respectively, which was sufficient to disentangle the shifted and unshifted components of the 132-keV  $2^+ \rightarrow 0^+$  transition of <sup>178</sup>Os. The mean recoil velocity  $v$  was found to be 0.76(2)% of the velocity of light  $c$ . A 0.7-mg/cm<sup>2</sup> self-supporting <sup>166</sup>Er target and a 6-mg/cm<sup>2</sup> Au stopper foil were used.

Because our experiment was especially tailored to determine the lifetime of the first  $2^+$  state in <sup>178</sup>Os, the second experiment was devoted to investigating the deorientation effect that is due to the hyperfine interactions [4] that affects RDDS measurements. The experimental setup was similar to that used in the RDDS experiment, but additional Ge detectors were used. In total, four detectors were positioned at angles of 0°, 55°, 108°, and 148° with respect to the beam axis. A 0.9-mg/cm<sup>2</sup> self-supporting <sup>166</sup>Er target and a 6-mg/cm<sup>2</sup> Au stopper were mounted into the plunger apparatus. Spectra were measured at nine different target-to-stopper distances: 0, 10, 30, 50, 100, 180, 250, 400, and 800 μm.

### III. DATA ANALYSIS AND RESULTS

#### A. Analysis of the delayed-coincidence data

The delayed-coincidence technique is a widely used tool for the determination of lifetimes of excited nuclear states down to the subnanosecond region. The normalized delayed-coincidence time distribution or time curve is given [5] by

$$F_i(t) = \int_{-\infty}^{\infty} P(t-x)f_i(x)dx, \quad (1)$$

where  $P$  is the prompt time distribution describing the response function of the setup and  $f_i$  is the probability for decay of the level of interest  $i$  at time  $x$ . Both  $P$  and  $f$  are normalized to unity.

Three basic methods for analyzing delayed-coincidence experiments are known and are widely applied to such data (see Ref. [6] and references therein). The convolution method is based on Eq. (1). By fitting the measured delayed time distribution, one can derive the different parameters associated with the function  $f_i(x)$ , including the lifetime  $\tau$  of the level of interest. Another method is based on the relations between the different moments of the delayed and prompt time distributions. Its most often used variant is the centroid-shift technique, which compares the first moments of the prompt and delayed time distributions to obtain the effective lifetime of the level of interest. If the feeding is prompt, the effective lifetime reduces to the lifetime of that level. As a third method, the slope of the delayed time distribution can be used for lifetime determination if the lifetime involved is, roughly speaking, larger than the FWHM of the prompt time distribution. Finally, we recently [7] developed a new procedure, which follows the approach of the differential decay-curve method (DDCM) [8,9] and allows a calculation of the mean lifetime  $\tau$  at every point of the measured time

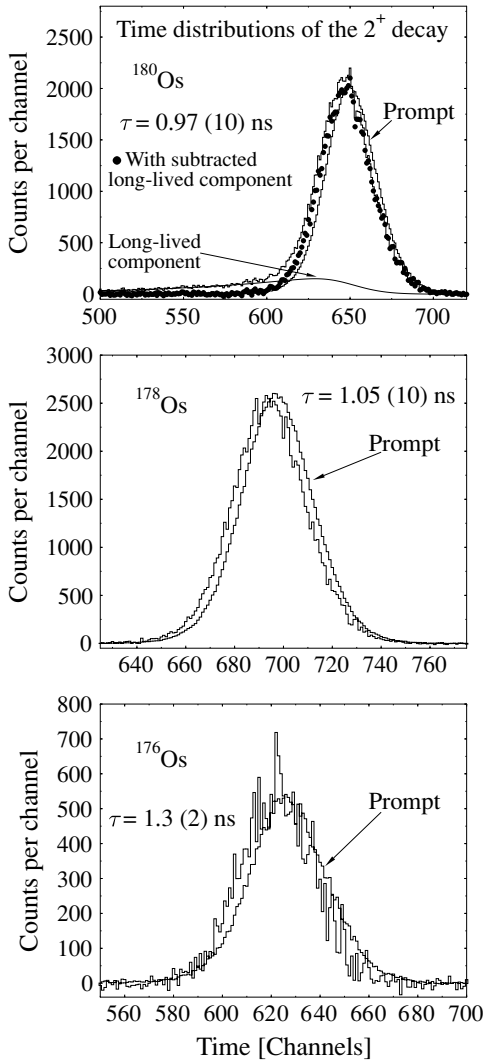


FIG. 1. Time distributions of the  $2^+ \rightarrow 0^+$   $\gamma$ -ray transitions in the Os isotopes studied compared with the corresponding normalized reference-time distribution. In the case of <sup>180</sup>Os, the subtraction of the long-lived component is also shown. The lifetimes derived by use of the centroid-shift technique are indicated.

curve. The final result for the lifetime is derived as an average over all calculated values. In the present work, we used for the analysis all these methods in order to obtain reliable and consistent results.

The first step in the analysis was to inspect the data for possible long-lived isomers. We achieved this by setting several gates on the time axis of the time- $\gamma$ -ray-energy matrices and investigating the relative behavior of the  $\gamma$ -ray intensities in the obtained prompt and delayed spectra. Inspection of these spectra reveals the existence of isomers with  $T_{1/2} \geq 2$  ns only in  $^{180}\text{Os}$  (see subsequent discussion). As a next step, the time distributions of transitions depopulating the levels of interest were obtained. For this purpose, gates were set on the energy axis of the matrices both on photopeaks and on neighboring regions of the Compton background. The time distributions corresponding to gates of the latter type were interpolated to obtain the contribution of the Compton background events to the time distributions corresponding to gates set on the photopeaks. This contribution was subtracted and, after elimination of the random coincidences, the resulting net time curves were further analyzed.

Prompt reference curves were obtained in two ways. For  $^{178,180}\text{Os}$ , we used the time distribution of the 136.3-keV  $\gamma$  ray originating from Coulomb excitation of Ta in the additional Ta foil mounted after the target. The energy of this  $\gamma$  ray is very close to the energies of the  $2_1^+ \rightarrow 0_1^+$  transitions, i.e., 132.4 keV in  $^{178}\text{Os}$  and 132.3 keV in  $^{180}\text{Os}$ , which means that the internal response function of the detector is the same. The lifetime,  $\tau = 57$  ps, of the depopulated level at 136.3 keV in  $^{181}\text{Ta}$  [10] is small compared with the time resolution of the setup. Because the effective feeding time, due to the cascades above the  $2_1^+$  level in  $^{178}\text{Os}$ , is almost the same [11], the feeding effect is compensated for in the final analysis. For  $^{176,180}\text{Os}$  we assumed the same effective feeding time as for  $^{178}\text{Os}$ , but for  $^{176}\text{Os}$  we did not use a Ta foil because the transition energy  $E_\gamma(2_1^+ \rightarrow 0_1^+) = 135.1$  keV is too close to the 136.3-keV transition energy in Ta and the peaks cannot be resolved. Therefore we used a different approach for the prompt reference. It was established that the prompt time distributions measured at different energies virtually coincide with the time distributions corresponding to the Compton background at the same energy. We checked this by plotting the centroid positions (first moments) of both sets of time distributions versus  $\gamma$ -ray energy. The time distributions of the transitions depopulating the  $2_1^+$  levels in  $^{176,178,180}\text{Os}$  are compared with the prompt time distributions in Fig. 1.

We obtained results for the lifetimes by utilizing all the aforementioned methods, which yielded consistent values in each case. In this way, for the lifetimes of the  $2_1^+$  levels we derive  $\tau(2_1^+ \text{ in } ^{176}\text{Os}) = 1.26$  (18) ns and  $\tau(2_1^+ \text{ in } ^{178}\text{Os}) = 1.05$  (10) ns.

In the case of  $^{180}\text{Os}$ , the analysis was complicated by the feeding from a higher-lying isomer. A partial level scheme of that nucleus is given in Fig. 2. Actually, four isomeric states were previously known [13]. In the present work, we did not observe the two higher-lying isomers with  $I \geq 20\hbar$  at 5848 keV [ $T_{1/2} = 12$  (4) ns] and  $I \geq 16\hbar$  [ $T_{1/2} = 41$  (10) ns], respectively. This is seemingly due to the different reaction.

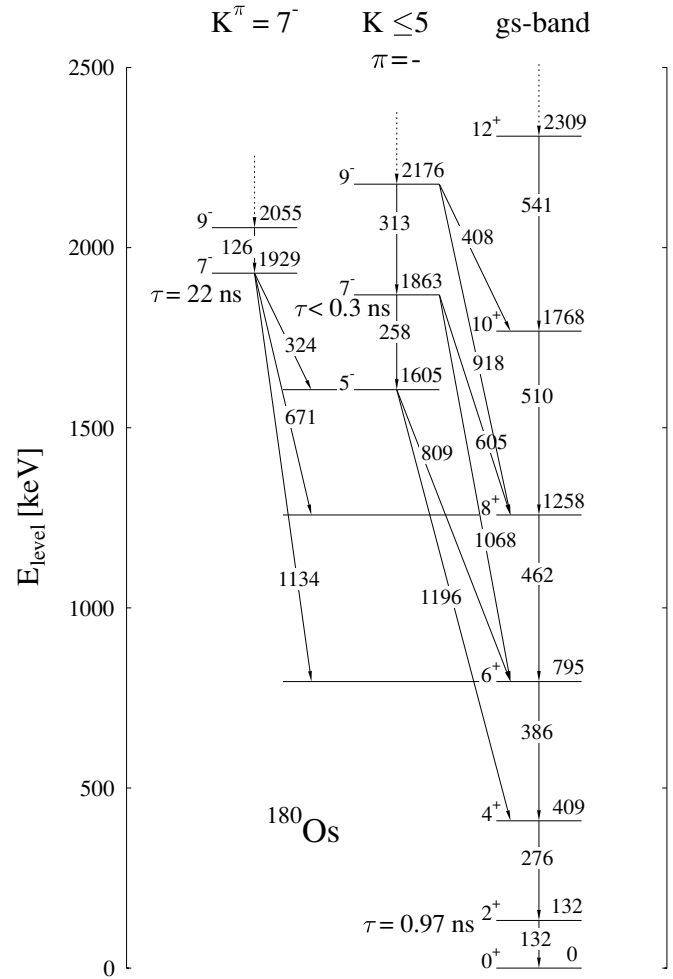


FIG. 2. Partial level scheme of  $^{180}\text{Os}$  taken from Ref. [12]. The level and  $\gamma$ -ray transition energies are given in kilo-electron-volts. The values of the derived lifetimes  $\tau$  are also indicated. gs: ground state.

In Ref. [13], the  $^{150}\text{Nd}(^{36}\text{S},6n)^{180}\text{Os}$  reaction at 177 MeV was used to populate excited states. The present measurement does not confirm the isomeric character of the  $I^\pi = 7^-$  state at 1863 keV. The centroid shift of the time distribution of the depopulating transition of 258 keV, compared with a prompt reference curve, sets only the limit  $\tau(1863 \text{ keV}) \leq 0.3$  ns. The fact that this state is not a long-lived isomer  $\{\tau = 25$  (4) ns, Ref. [13] $\}$  is also confirmed by the analysis of the time distributions of the transitions within the ground-state band (gsb) starting from spin  $I = 8\hbar$  and below. These distributions possess prompt and slow components, the latter of which can be fully explained with the feeding from the  $I^\pi = 7^-$  isomer at 1929 keV. Additional long-lived feeding from higher-lying levels, including the level at 1863 keV, was not revealed. The lifetime ( $\tau = T_{1/2}/\ln 2$ ) of the level at 1929 keV was first determined as  $\tau = 23$  (3) ns in Ref. [14]. A later work [13] resulted in a different value,  $\tau = 38$  (4) ns. The value adopted in the *Nuclear Data Sheets* is 35 (6) ns [12]. However, the present work supports the earlier result of Ref. [14].

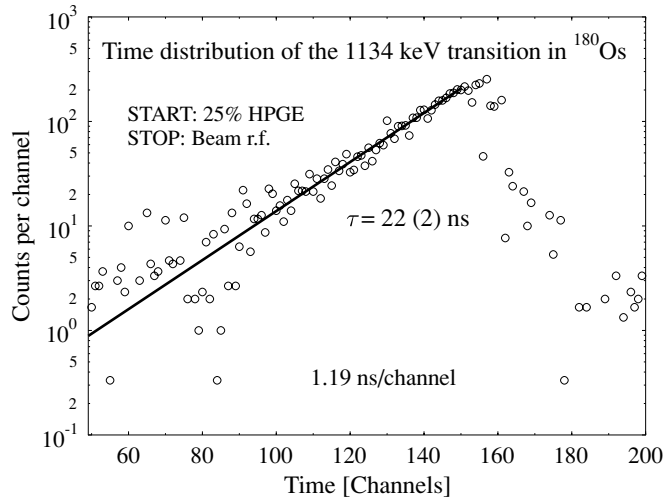


FIG. 3. Decay of the  $I^\pi = 7^-$  isomer at 1929 keV in  $^{180}\text{Os}$  (see also Fig. 2 and text). The start signal for the time-to-amplitude convertor was provided by a high-purity Ge (HPGe) detector with 25% efficiency.

This finding is based on the following evidence. First, in Fig. 3, the time distribution of the 1134-keV transition depopulating the level at 1929 keV is displayed. The fit of the slope yields  $\tau = 22$  (3) ns. Second, a similar value is extracted from the long-lived components of the time distributions of the transitions within the gsb. To determine the lifetime of the  $2_1^+$  level, the long-lived component was subtracted according to a procedure we applied earlier [15]. The procedure consists, on the basis of known prompt time distribution and structure of the function  $f$  describing the decay of the level of interest [see Eq. (1)], of a calculation of the long-lived component and its fit to the data. This component is shown in Fig. 1 as well as the prompt reference curve and the sum of the two composing components (i.e., the measured data). The centroid analysis yields  $\tau = 0.97$  (10) ns, which is close to the previously measured [16] value  $\tau = 1.15^{+0.30}_{-0.20}$  obtained with the RDDS technique. The present result is, however, characterized by smaller error bars.

### B. Analysis of the RDDS and deorientation data

The RDDS technique exploits the fact that the splitting of the intensity of a  $\gamma$ -ray transition into shifted and unshifted components depends on the distance  $x$  between the target and the stopper. The Doppler-shifted component is associated with decays during the flight in vacuum of the recoiling nucleus whereas the unshifted component corresponds to decays occurring after coming to rest in the stopper. The evolution of that splitting with the target-to-stopper distance can be used for a lifetime determination if the feeding from higher-lying levels is taken into account. Details on the RDDS technique and the traditional procedures for data analysis can be found in Ref. [17] and references therein.

The spectra taken at different distances were first normalized using lines arising from Coulomb excitation of the nuclei of the Au stopper. Then, with a careful fitting procedure,

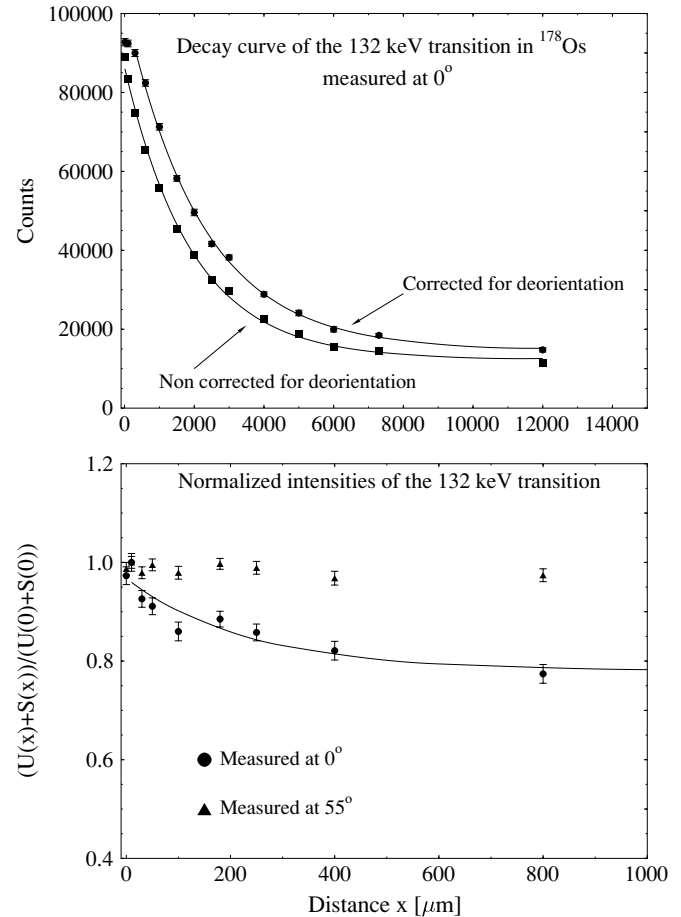


FIG. 4. Upper panel: Decay curve of the unshifted component of the 132-keV transition measured at the angle of  $0^\circ$  without (squares) and with (circles) a correction for the deorientation effect. The curves drawn correspond to a fit that takes into account the effective feeding. Lower panel: Total normalized intensities, i.e., sums of the unshifted (U) and shifted (S) components of the 132-keV transition measured at angles of  $0^\circ$  and  $55^\circ$ .

the unshifted and shifted components of the transition were determined. Only the intensities of the unshifted components were used for the lifetime analysis. The unshifted component of the 132-keV transition (or the decay curve) derived in this way is indicated by filled squares in the upper panel of Fig. 4. We note that, because of the relatively large target thickness, about 10% of the recoils do not leave the target and contribute to the unshifted peak even at the largest distances. This effect was confirmed by both a Monte Carlo simulation of the process of creation and slowing down of the recoils in the target and by a measurement in which only a target foil was used without a stopper. A simple fit of the decay curve with the effective feeding time taken into account yields a value of about 0.90 (7) ns for the lifetime of the  $2_1^+$  level. The discrepancy of this result with what is obtained in the delayed coincidence measurement is approximately 15% (see Sec. III A,  $\tau = 1.05$  ns). The reason for this is the deorientation effect, which leads to a loss of nuclear alignment during the flight in vacuum that is due to the hyperfine interactions (see, e.g., Ref. [4] and references therein). Thus the alignment undergoes an

TABLE II. Lifetimes and reduced transition probabilities  $B(\sigma L)$  in units of  $e^2 b^L$  and Weisskopf units (W.u.) as derived in the present work. The branching ratios and measured internal conversion coefficients necessary to calculate the transition strengths are taken from Ref. [12].

Nucleus	$E_{\text{level}}$ (keV)	$\tau$ (ns)	$E_\gamma$ (keV)	$I^{\pi_i}$	$I^{\pi_f}$	$\sigma L$	$B(\sigma L)$	$B(\sigma L)$ (W.u.)
$^{176}\text{Os}$	135.1	1.21 (18)	135.1	$2^+$	$0^+$	$E2$	0.632 (98)	108 (17)
$^{178}\text{Os}$	132.4	0.99 (7)	132.4	$2^+$	$0^+$	$E2$	0.820 (60)	138 (10)
$^{180}\text{Os}$	132.3	0.97 (10)	132.3	$2^+$	$0^+$	$E2$	0.837 (90)	139 (15)
	1862.9	$1.15^{+0.30}_{-0.20}$ <sup>a</sup> <0.3	101.4	$7^-$	$6^-$	$(E2)^b$	>0.33	>55
			235.3		$(6)^+$	$(E1)$	$>0.9 \times 10^{-7}$	$>0.4 \times 10^{-5}$
			258.0		$5^-$	$E2$	>0.062	>10
			483.4		$6^+$	$E1$	$>2.5 \times 10^{-8}$	$>1.2 \times 10^{-6}$
			604.9		$8^+$	$E1$	$>3.8 \times 10^{-8}$	$>1.8 \times 10^{-6}$
			1067.5		$6^+$	$(E1)$	$>3.5 \times 10^{-10}$	$>1.7 \times 10^{-8}$
	1929.1	22 (2)	51.9	$7^-$	$6^+$	$E1$	$7.6(1.0) \times 10^{-7}$	$3.7(0.5) \times 10^{-5}$
			324.4		$5^-$	$E2$	$1.4(0.3) \times 10^{-4}$	0.023(5)
			671.1		$8^+$	$(E1)$	$1.2(0.3) \times 10^{-10}$	$5.8(1.5) \times 10^{-9}$
			1133.8		$6^+$	$(E1)$	$3.7(0.8) \times 10^{-11}$	$1.8(0.4) \times 10^{-9}$

<sup>a</sup>Ref. [19]

<sup>b</sup>If  $M1, B(M1) > 2.3 \times 10^{-3} \mu_N^2$  ( $1.3 \times 10^{-3}$  W.u.)

evolution with time, which modifies the angular distribution of the emitted  $\gamma$  rays and a complementary time dependence is superimposed on the normally expected time behavior of the intensities.

We investigated the deorientation effect with the measurement described in the previous section. Experimentally, the technique applied is very close to the RDDS one. To study the effect quantitatively, it is necessary to disentangle the shifted and unshifted components of a transition at different detector angles and determine the angular distribution function that undergoes an evolution with time  $t$  (distance  $x = vt$ ). The unshifted components are more suitable for such investigations, as the perturbations leading to the deorientation are usually considered to be frozen when the recoil enters the stopper. Therefore the angular distribution of this component yields directly the attenuation coefficients describing the loss of alignment (see, e.g., Ref. [18]). In the present case, the situation was simplified by the fact that the 132-keV transition does not have a shifted component until a distance of flight of 600  $\mu\text{m}$ . Therefore the sum of the unshifted and shifted components is practically dominated by the unshifted component until the end of this distance range. On the other hand, this sum or total intensity should remain constant at different distances. In the lower panel of Fig.4, the total intensities of the 132-keV transition are presented as measured at the angles of  $0^\circ$  and  $55^\circ$  and normalized to the smallest distance. The decrease of the intensity in the first 200–400  $\mu\text{m}$  at  $0^\circ$  is due to the deorientation effect. Because at  $55^\circ$  the Legendre polynomial  $P_2 \approx 0$ , here the effect is weakly felt and the total intensity remains constant. Similarly, we investigated the decay curves of the  $4_1^+ \rightarrow 2_1^+$  transition of 266 keV at different angles. For this transition, a better separation of the unshifted and shifted components can be achieved even at angles larger than  $0^\circ$ . It was established that the  $4_1^+$  level is also influenced by the deorientation. Therefore, because of the deorientation at the  $4_1^+$  and  $2_1^+$  levels, with higher spin levels of the gsb not contributing to this effect [18], a loss of alignment at the

$2_1^+$  level occurs. For the decay curve measured at  $0^\circ$  shown in Fig. 4, this leads to a decrease of the intensity because at this angle the  $\Delta I = 2$   $E2$  transitions are enhanced by the alignment.

To correct the decay curve of the 132-keV transition determined in the RDDS experiment by using the detector at  $0^\circ$ , we performed the following steps. First, a simple function  $f(x) = ae^{-x/b} + c$  was fitted to the normalized decay curve of the total intensity obtained from the deorientation experiment at the angle  $0^\circ$ . The fit is also shown in Fig. 4, lower panel. The noncorrected decay curve (from the RDDS experiment) in the upper panel of Fig. 4 was divided by this function to obtain a corrected decay curve that is also indicated in the upper panel by circles. A simple fit of this corrected decay curve with the effective feeding taken into account yields for the lifetime of the  $2_1^+$  level a value  $\tau = 0.94$  (9) ns, which is very close to the result obtained in the delayed-coincidence experiment [ $\tau = 1.05$  (10) ns]. As a final value of the lifetime of the  $2_1^+$  level in  $^{178}\text{Os}$  we adopt  $\tau = 0.99$ (7) ns, which is an average of the results from the delayed-coincidence and RDDS measurements. The agreement between the results from these two measurements obtained with different methods supports the reliability of the lifetimes derived in the present work.

#### IV. DISCUSSION

The lifetimes determined in the present work and the corresponding electromagnetic transition strengths are presented in Table II. Using our data and results compiled in the *Nuclear Data Sheets* for the even-even Os isotopes with  $A = 172\text{--}192$ , we derived from the  $B(E2, 2_1^+ \rightarrow 0_1^+)$  transition strength the experimental quadrupole deformation  $\beta_2$  of these nuclei, which is presented in Table III. For this purpose, the well-known formula [1]

$$B(E2, I \rightarrow I - 2) = \frac{5}{16\pi} Q_0^2 (2020|00)^2 \quad (2)$$

TABLE III. Quadrupole deformations  $\beta_2$  (and their experimental uncertainties) of the ground states of the even-even Os isotopes.

$A$	172	174	176	178	180	182
$\beta_2$	0.196(7)	0.227(13)	0.185(14)	0.209(7)	0.210(11)	0.201(4)
$A$	184	186	188	190	192	
$\beta_2$	0.183(4)	0.171(3)	0.163(3)	0.155(3)	0.147(2)	

was first applied to extract the quantity  $Q_0$  that, in the framework of the rigid-rotor model, coincides with the intrinsic quadrupole moment. Then the deformation  $\beta_2^o$  of the nuclear charge distribution was derived with the expression [20]

$$Q_0 = \frac{3}{\sqrt{5\pi}} Z R_0^2 \beta_2^o (1 + 0.16\beta_2^o). \quad (3)$$

Although this derivation is somewhat model dependent, it makes it possible to compare the quadrupole deformations of different nuclei and is widely used. The quadrupole deformation  $\beta_2$  in Table III characterizes the nuclear mean field and was obtained according to the prescription of Ref. [21], by decreasing  $\beta_2^o$  with a factor of 1.1.

To give the characteristics of the evolution of the collectivity in the even-even Os isotopes in condensed form, we present in Fig. 5 two experimentally derived quantities. The top panel of the figure illustrates the behavior of the ratio of the energies of the  $4_1^+$  and  $2_1^+$  states. This ratio varies between the values of 2.0, for a perfect vibrational nucleus, and 3.33 for an axially symmetric rotational nucleus. The systematic values for the Os nuclei tend toward the rotational limit and attain their maximum at  $N = 108$ , which is just after the midshell.

However, the nuclear deformation  $\beta_2$  has a maximum just around midshell, as illustrated in the bottom panel of Fig. 5. This phase-retardation feature between the maxima of the rotationlike behavior of the energy levels and the quadrupole deformation  $\beta_2$  extracted from the  $B(E2, 2_1^+ \rightarrow 0_1^+)$  transition strengths is very interesting but cannot be explained by simple phenomenological models. A maximum deformation at midshell strongly supports the simple Interacting Boson Approximation (IBA) interpretation of the quantity  $N_\pi N_\nu$  as a parameter controlling the collectivity [2]. We remind the reader that this quantity is the product of the numbers of valence protons and valence neutrons.

It should be mentioned that the experimental  $\beta$  deformation of  $^{174}\text{Os}$  does not follow a simple systematic trend: instead of the expected slowly decreasing behavior when going toward the  $N = 82$  closed shell, a zigzaglike picture is observed. Whether this zigzag behavior is based on real structural effects or caused only by experimental problems cannot be answered at this stage. Unfortunately the experimental errors of the  $\beta$  values for  $^{174,176}\text{Os}$  are relatively large compared with the uncertainties of these quantities for the neighboring Os nuclei. Therefore it would be of interest to remeasure the corresponding  $2^+$  lifetimes more precisely. The confirmation of the actual results would reveal strong structural effects on the observed nuclear deformations at neutron numbers  $N = 96$ –100. Such effects, if existing, would be beyond a

description with a smooth function of the product of valence proton and neutron numbers  $N_\pi N_\nu$ .

Many theoretical calculations in the literature have been devoted to the even-even Os isotopes and especially to the description of the quadrupole deformation and the related  $B(E2, 2_1^+ \rightarrow 0_1^+)$  transition strengths. In Fig. 6, the data on the transitions strengths in these nuclei are compared only with theories that predict values throughout the whole isotopic chain [21–23] and come close to the experimental features. Other thorough calculations [24–26] have been also considered, but they provide a worse description of the data than the calculations presented in Fig. 6. The theoretical

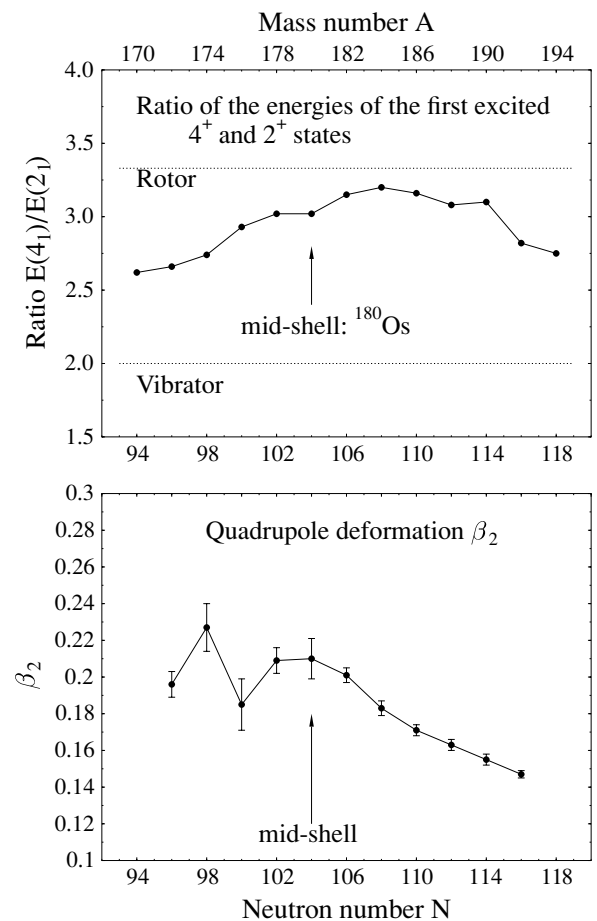


FIG. 5. Different aspects of the development of the collectivity in the even-even Os isotopes. The upper panel of the figure shows the ratio of the energies of the  $4_1^+$  and  $2_1^+$  states. In the lower panel, the values of the quadrupole deformation are displayed for the different isotopes. In all panels, the solid lines are drawn to guide the eye.

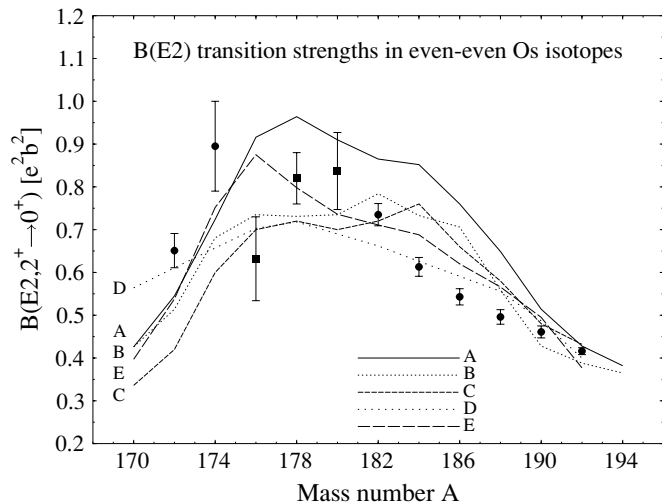


FIG. 6. Experimental  $B(E2, 2_1^+ \rightarrow 0_1^+)$  transition strengths compared with different theoretical calculations. The values derived in the present work for  $^{176-180}\text{Os}$  are indicated by filled squares. The experimental data for the other nuclei, which are represented by filled circles, are taken from the *Nuclear Data Sheets*. The theoretical values are taken as follows: A from Ref. [21], B from Ref. [22], and C–E from the compilation of Raman, Nestor, and Tikkanen [23] (see also text).

curve (A) is taken from the work of Nazarewicz, Riley, and Garrett [21], in which equilibrium nuclear deformations were calculated by use of the shell-correction method with an average Woods-Saxon potential and a monopole pairing residual interaction. This curve describes qualitatively the data, and the discrepancy with respect to the reproduction of the absolute values might be compensated for by a scaling factor. Möller and Nix calculated [22] nuclear masses and deformations by using a mass formula based on a Yukawa-plus-exponential macroscopic model and a folded-Yukawa microscopic model. In Fig. 6, their results for the Os isotopes investigated are indicated by curve B. They give a reasonable description of the data but fail to reproduce the decrease of the  $B(E2)$  values in  $^{184-188}\text{Os}$ . The same features characterize the “global best fit” from the compilation of Raman *et al.* [23], which is represented by curve C. The predictions of the single-shell asymptotic Nilsson model from the same compilation, represented by curve D, describe the heavier isotopes better, but fail to reproduce in a completely correct way the maximum of the experimental data around midshell. The same holds also for the calculation made with the Woods-Saxon model in the compilation of Raman *et al.* [23] (curve E). Although the models considered provide a reasonable overall description of the data, in some cases within the error

bars, further efforts are needed to reproduce the details, and especially the maximum at midshell, which finds a simple explanation in the framework of the IBA. This feature needs justification on a microscopic or a semimicroscopic level as well.

Concerning the transition strengths measured for the two  $I^\pi = 7^-$  levels in  $^{180}\text{Os}$ , it can be mentioned that the new lifetime value of  $\tau = 22$  ns does not affect the interpretation [14] of the level at 1929 keV as a high  $K = 7$  isomer based on a two-quasi-neutron configuration, most probably  $7/2^+[633] + 7/2^-[514]$ , with a small two-quasi-proton admixture. However, for the level at 1863 keV, the new limit for the lifetime (see Table II) does not support the interpretation of this level given in Ref. [13] as another high- $K$  isomer and bandhead. Our result is consistent with that of Ref. [14], in which this level is assigned as member of a low- $K$  two-quasiparticle band, probably containing octupole admixtures at lower spins. Simple two-band mixing considerations for these two  $I^\pi = 7^-$  levels lead to an estimate of the interaction strength of  $V \leq 2-3$  keV, which could be due to  $K$  mixing. This interaction is sufficient to explain the  $B(E2)$  strength of the transition from the isomeric  $I^\pi = 7^-$  level at 1929 keV to the  $I^\pi = 5^-$  level at 1605 keV belonging to the low- $K$  negative-parity band.

## V. CONCLUSIONS

The lifetimes of the first excited  $2^+$  states in  $^{176,178}\text{Os}$  have been measured for the first time with the pulsed-beam technique. With the same technique, the lifetime of the  $2_1^+$  level in  $^{180}\text{Os}$  was determined with a better precision, as were the lifetimes of two higher-lying  $I^\pi = 7^-$  isomers in that nucleus. A recoil-distance Doppler-shift experiment for  $^{178}\text{Os}$  was carried out to cross-check the results obtained with the pulsed-beam method. The result of the RDDS measurement was corrected for the nuclear deorientation effect, which was measured directly in an extra experiment. With the newly determined lifetimes, the  $B(E2, 2_1^+ \rightarrow 0_1^+)$  transition strengths in the even-even Os isotopes show a maximum at midshell for  $N = 104$ , which finds a simple explanation by the  $N_\pi N_\nu$  rule of the IBA but requires new theoretical calculations for its description within the framework of microscopic models.

## ACKNOWLEDGMENTS

The authors are indebted to S. F. Ashley for carefully reading the manuscript. P. P. is grateful for the kind hospitality of the colleagues at the University of Cologne. This work was supported by the Bundesministerium für Bildung, Forschung und Technologie (Germany) under contract no. 06K167.

- [1] A. Bohr and B. R. Mottelson, *Nuclear Structure* (Benjamin, New York, 1975), Vol. 2.
- [2] R. F. Casten, *Nucl. Phys.* **A443**, 1 (1985).
- [3] A. Dewald *et al.*, in *Proceedings of the '98 Seminar on Nuclear Physics with Radioactive Ion Beam and High Spin Nuclear*

*Structure*, edited by G. Jin, Y. Luo, and W. Zhan (Atomic Energy Press, Lanzhou, China, 1998), p. 31.

- [4] G. Goldring, in *Heavy Ion Collisions*, edited by R. Bock (North-Holland, Amsterdam, 1982), Vol. 3, p. 484.
- [5] T. D. Newton, *Phys. Rev.* **78**, 490 (1950).

- [6] K. P. Lieb, in *Experimental Techniques in Nuclear Physics*, edited by D. N. Poenaru and W. Greiner (de Gruyter, Berlin/New York, 1997), p. 425.
- [7] P. Petkov, O. Möller, D. Tonev, A. Dewald, and P. von Brentano, *Nucl. Instrum. Methods Phys. Res. A* **500**, 379 (2003).
- [8] A. Dewald, S. Harissopulos, and P. von Brentano, *Z. Phys. A* **334**, 163 (1989).
- [9] G. Böhm, A. Dewald, P. Petkov, and P. von Brentano, *Nucl. Instrum. Methods Phys. Res. A* **329**, 248 (1993).
- [10] R. B. Firestone, *Nucl. Data Sheets* **62**, 101 (1991).
- [11] A. Dewald *et al.*, *J. Phys. G* (to be published).
- [12] E. Browne, *Nucl. Data Sheets* **71**, 81 (1994).
- [13] Ts. Venkova, T. Morek, G. V. Marti, H. Schnare, A. Krämer-Flecken, W. Gast, A. Georgiev, G. Hebbinghaus, R. M. Lieder, G. Sletten, K. M. Spohr, K. H. Maier, and W. Urban, *Z. Phys. A* **344**, 417 (1993).
- [14] G. D. Dracoulis, C. Fahlander, and M. P. Fewell, *Nucl. Phys. A* **383**, 119 (1982).
- [15] P. Petkov, W. Andrejtscheff, S. J. Robinson, U. Mayerhofer, T. von Egidy, S. Brant, V. Paar, and V. Lopac, *Nucl. Phys. A* **554**, 189 (1993).
- [16] R. Kaczarowski, U. Garg, A. Chaudhury, E. G. Funk, J. W. Mihelich, D. Frekers, R. V. F. Janssens, and T. L. Khoo, *Phys. Rev. C* **41**, 2069 (1990).
- [17] T. K. Alexander and J. S. Forster, *Adv. Nucl. Phys.* **10**, 197 (1978).
- [18] P. Petkov, A. Dewald, A. Gelberg, G. Böhm, P. Sala, P. von Brentano, and W. Andrejtscheff, *Nucl. Phys. A* **589**, 341 (1995).
- [19] S.-C. Wu and H. Niu, *Nucl. Data Sheets* **100**, 483 (2003).
- [20] A. Bohr and B. R. Mottelson, *Dan. Mat.-Fys. Medd.* **30**, 1 (1955).
- [21] W. Nazarewicz, M. A. Riley, and J. D. Garrett, *Nucl. Phys. A* **512**, 61 (1990).
- [22] P. Möller and J. R. Nix, *At. Data Nucl. Data Tables* **26**, 165 (1981).
- [23] S. Raman, C. W. Nestor Jr., and P. Tikkanen, *At. Data Nucl. Data Tables* **78**, 1 (2001).
- [24] U. Götz, H. C. Pauli, K. Alder, and K. Junker, *Phys. Lett.* **B38** 274 (1972).
- [25] B. Nerlo-Pomorska, *Z. Phys. A* **293**, 9 (1979).
- [26] P. Möller, W. D. Meyers, and W. J. Swiatecki, *At. Data Nucl. Data Tables* **59**, 185 (1995).